

Calculation of Special Spin Behavior of Dy³⁺ in DyFe_{1-x}Cr_xO₃ System by Molecular Field Model

Kaiyang Gao¹, Kexuan Zhou¹, Jiyu Shen¹, Zeyi Lu¹, Chenying Gong¹, Zhongjin Wu¹,
Ke Shi¹, Jing Guo¹, Zhaoyi Wang³, Min Liu^{*,1,2}

¹College of Nuclear Science and Technology, University of South China, Hengyang 421200, Hunan, P.R China.

²Zhuhai Tsinghua University Research Institute Innovation Center, 101 University Ave, Tangjiawan Zhuhai 519000, P.R China.

³College of physics and Electronic Sciences, Hunan Normal University, Changsha 410081, Hunan, P.R China.

Email: liuhart@126.com, xiayfusc@126.com

Abstract

In this study, the sol-gel method synthesized the magnetic measurement and analysis of single-phase polycrystalline perovskite DyFe_{1-x}Cr_xO₃ (DFCO). The experimental data were fitted and calculated by a four-sublattice molecular field model. Unlike previous studies, we found that in DyFe_{1-x}Cr_xO₃, the spin of the A-site rare earth ion Dy³⁺ also changed simultaneously with the spin reorientation of the Fe³⁺/Cr³⁺ ions. The effective spin is defined as the projection of the A site's total spin on the B site's spin plane, and the curve of temperature changes is obtained after fitting. With this theory, a very accurate thermomagnetic curve is obtained by fitting. This is convincing and, at the same time, provides a reference for the development of spintronic devices in the future.

Keywords : DyFe_{1-x}Cr_xO₃; magnetism; spin reorientations; molecular field model; mössbauer.

Introduction

Rare earth-based perovskites have always been critical raw materials for information storage devices and read/write heads [1,2] and are also widely studied as magneto-optical effects. [3-6] This is attributed to the rich and complex magnetism of this class of materials; especially after the addition of rare earth ions with a net magnetic moment, the source of their magnetic nature will become very complex. In the past few years, many scholars have done exciting research on it. Wu et al. [7] reported that the twofold spin reorientation behavior of the double rare earth orthoferrite $\text{Dy}_{0.5}\text{Pr}_{0.5}\text{FeO}_3$ originated from the effective anisotropic field generated by the R^{3+} ion spin interaction and could be controlled by an external magnetic field. Park et al. [8] calculated by density functional and dynamical mean field theory that the metal-insulator transition of Rare-earth-element nickelates originates from the site-selective Mott phase. Najee et al. [9] recently demonstrated direct, reversible, and continuous control of the ferromagnetism of rare-earth titanium-based perovskites by uniaxial strain affecting the tilt and rotation of TiO_6 octahedra.

DyFe/CrO_3 is a typical perovskite whose magnetic properties consist of complex exchange interactions due to the presence of two transition metal ions at the B site: $\text{Dy}^{3+}\text{-Dy}^{3+}$, $\text{Dy}^{3+}\text{-Fe}^{3+}$, $\text{Dy}^{3+}\text{-Cr}^{3+}$, $\text{Fe}^{3+}\text{-Fe}^{3+}$, $\text{Cr}^{3+}\text{-Cr}^{3+}$, $\text{Fe}^{3+}\text{-Cr}^{3+}$. In general, up to the Néel phase transition temperature of $\text{Fe}^{3+}\text{-Fe}^{3+}/\text{Cr}^{3+}\text{-Cr}^{3+}$ (approximately 650 K to 750 K for Fe and 120 K to 300 K for Cr) [10.11], the overall magnetism of the system is directly contributed by the G-type antiferromagnetic structure of $\text{Fe}^{3+}/\text{Cr}^{3+}$. At the ultra-low temperature of around 5 K, [12] the magnetic moment of $\text{Dy}^{3+}\text{-Dy}^{3+}$ is fixed

to the ordered structure, and a firm antiferromagnetic order appears. Still, above 5 K temperature, it only contributes to a strong paramagnetism.

In most rare earth perovskite, there is a particular spin orientation behavior - spin reorientation. This spintronics phenomenon originates from the strong coupling between the high-spin rare earth ion (4f) and the transition metal ion (3d). In many previous studies, the spin reorientation behavior of B-site ions has been investigated by growing single crystals and attaching external magnetic fields in different easy-axis directions. [13-15] However, very little research has been done on magnetic simulation.

This study uses the four-lattice molecular field theory to perform a magnetic fit to a polycrystalline DFCO system. It is found that not only do the transition metal ions at the B-site undergo a spin orientation transition during thermogenic spin reorientation, but also the A-site rare earth ions undergo a similar continuous spin change simultaneously. Finally, the values of the exchange constants and the effective spins, closely related to the macroscopic magnetism, are obtained. This approach has been studied with excellent results in other partial rare earth perovskite systems. [16-19]

Experimental

Sample Preparation

$\text{DyFe}_{1-x}\text{Cr}_x\text{O}_3$ ($x=0.1$ and 0.9) was prepared by a simple sol-gel combustion method. The required precursors are all from McLean, namely Dysprosium nitrate ($\text{Dy}(\text{NO}_3)_3 \cdot 6\text{H}_2\text{O}$), iron nitrate nonahydrate ($\text{Fe}(\text{NO}_3)_3 \cdot 9\text{H}_2\text{O}$), chromium nitrate

nonahydrate ($\text{Cr}(\text{NO}_3)_3 \cdot 9\text{H}_2\text{O}$), ethylene glycol ($\text{C}_2\text{H}_6\text{O}_2$), citric acid ($\text{C}_6\text{H}_8\text{O}_7$). First, all nitric acid compounds were mixed and dissolved in deionized water according to a certain ion ratio ($\text{Dy}^{3+} : \text{Fe}^{3+} : \text{Cr}^{3+} = 1 : 0.1/0.9 : 0.9/0.1$). Then, the excess citric acid and a certain amount of ethylene glycol are mixed in a molar ratio of 1:1. Stir the solution uniformly on a magnetic stirrer at 80 °C until a gel form. Then, heat the gel to 120 °C. The resulting powder was pre-calcined at 600 °C for 12 h, then calcined at 1200 °C for 24 h, and cooled to obtain the final nanopowder sample.

X-ray diffraction measurements (XRD)

X-ray diffraction (XRD) experiments were carried out in Siemens D500 Cu $K\alpha$ ($\lambda = 1.5418 \text{ \AA}$) diffractometer with the range of 20° to 80° (rate of 0.02°/s). The obtained data were processed with Fullprof software.

Mössbauer spectrum Test

The transmission ^{57}Fe Mössbauer spectrum of $\text{DyFe}_{1-x}\text{Cr}_x\text{O}_3$ ($x=0.1$ and 0.9) were collected at 300 K on SEE Co W304 Mössbauer spectrometer with a $^{57}\text{Co}/\text{Rh}$ source in transmission geometry equipped in a cryostat (Advanced Research Systems, Inc., 4 K). The data results were fitted with MössWinn 4.0 software.

Magnetic Measurement

The thermomagnetic curves (M-T) of the $\text{DyFe}_{1-x}\text{Cr}_x\text{O}_3$ ($x=0.1$ and 0.9) were obtained in the external field of 100 Oe and the temperature in the range of 10 K to

400 K. And the magnetization curves (M-H) under -7 T to 7 T magnetic field were measured at 300 K temperature.

Results and discussions

XRD analysis

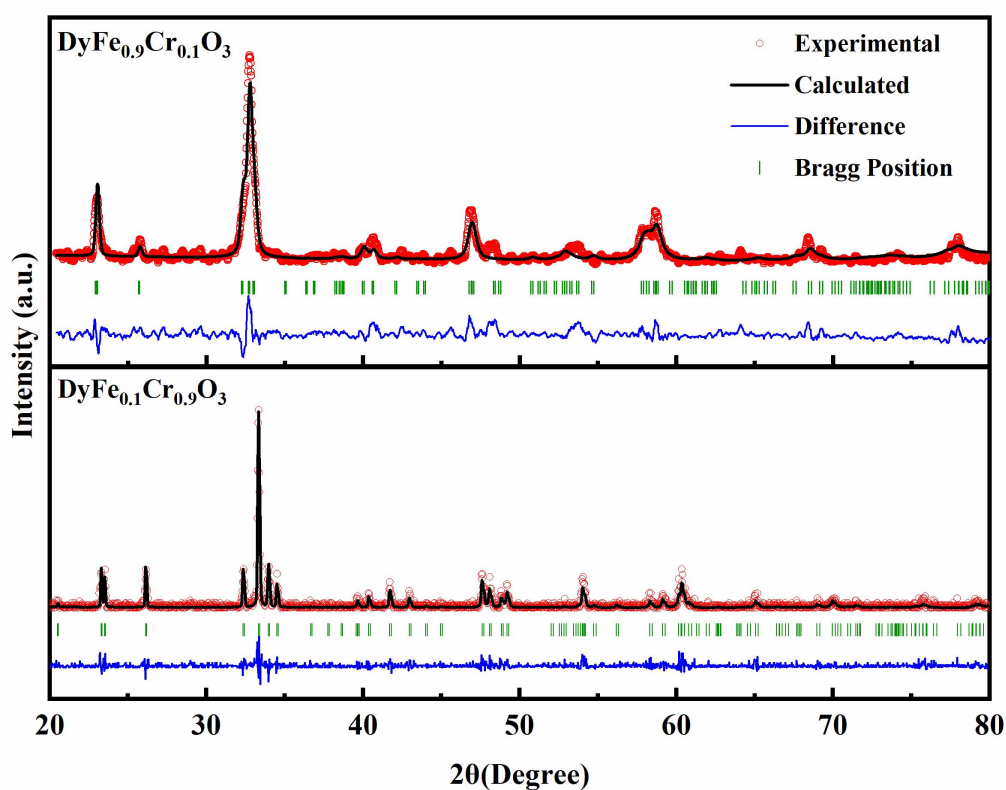


Fig. 1. The refined XRD patterns of $\text{DyFe}_{1-x}\text{Cr}_x\text{O}_3$ ($x=0.1$ and 0.9).

Table. 1. The refined lattice parameters and unit cell volume of $\text{DyFe}_{1-x}\text{Cr}_x\text{O}_3$ ($x=0.1$ and 0.9).

Sample	a (Å)	b (Å)	c (Å)	Cell Volume (Å ³)	ASD (%)
$\text{DyFe}_{0.9}\text{Cr}_{0.1}\text{O}_3$	5.5967	7.6334	5.3134	227.0006	0

Figure. 1 shows the XRD patterns of DyFe_{1-x}Cr_xO₃ (x=0.1 and 0.9) refined by Fullprof software. Both samples exhibited good crystallinity and only had a single-phase structure, in which DyFe_{0.9}Cr_{0.1}O₃ belonged to the orthorhombic *Pbnm* space group, and DyFe_{0.1}Cr_{0.9}O₃ belonged to the orthorhombic *Pnma* space group. It is not difficult to see that when the Cr doping amount increases, although the architecture maintains the orthogonal perovskite type, its orthogonal symmetry has changed greatly. The structural parameter (D_{OD}) is introduced to characterize the orthogonal distortion in the following formula: [20]

$$D_{OD} = \frac{1}{3} \sum_{i=1}^3 \left| \frac{\alpha_i - \bar{\alpha}}{\bar{\alpha}} \right| * 100\% \#(1)$$

For the lattice of the *Pbnm* space group, $\alpha_1 = a$, $\alpha_2 = b$, $\alpha_3 = c/\sqrt{2}$, $\bar{\alpha} = (a * b * c/\sqrt{2})^{\frac{1}{3}}$. And for *Pnma* space group, $\alpha_1 = c$, $\alpha_2 = a$, $\alpha_3 = b/\sqrt{2}$, $\bar{\alpha} = (a * b * c/\sqrt{2})^{\frac{1}{3}}$.

The lattice constant, unit cell volume, and anti-site defect factor (ASD) are presented in Table 1. A rough ASD value can be obtained by Fullprof refinement, indicating the ratio of Fe/Cr ions on the B site to occupy each other. According to the refinement results of these two samples, we calculated that their ASD values are basically 0 %. This is because in the case of large ratio differences, the dopant ions will only occupy the lowest energy positions. A large ASD value occurs only when the B-site Fe/Cr ion ratios are close to or even the same, as in our previous study of NdFe_{0.5}Cr_{0.5}O₃. [9] As Cr ions far exceed Fe ions, both the lattice constant and the unit

cell volume decrease accordingly. This is enough to see the effect of ionic radius on it.

[19, 21]

Mössbauer spectrum and Magnetization curve analysis

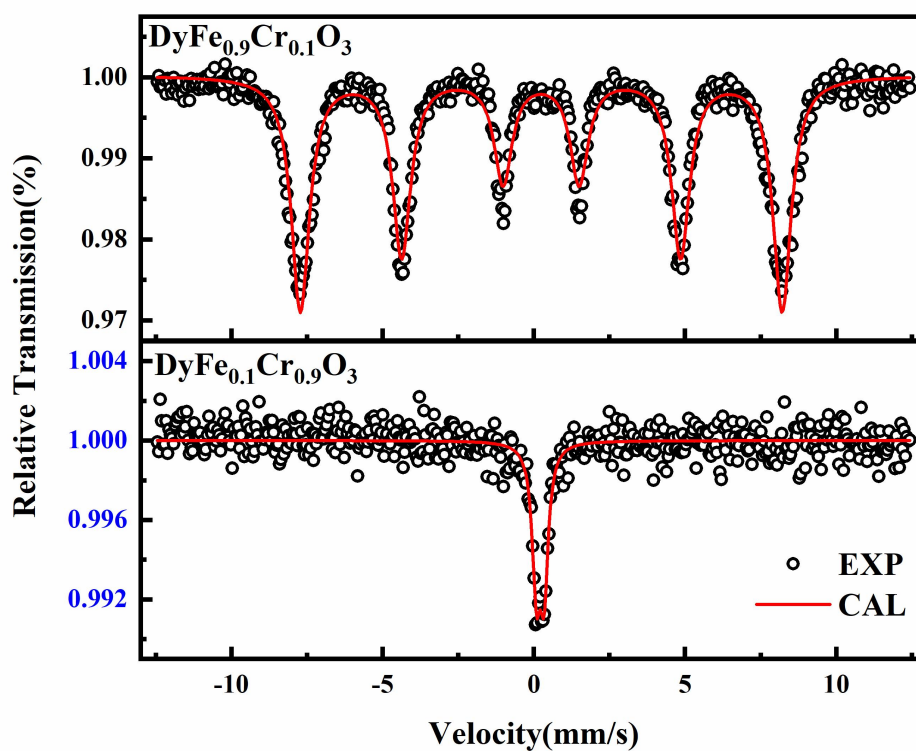


Fig. 2. Mössbauer spectrum of $\text{DyFe}_{1-x}\text{Cr}_x\text{O}_3$ ($x=0.1$ and 0.9) at 300 K.

Table. 2. Hyperfine parameters of $\text{DyFe}_{1-x}\text{Cr}_x\text{O}_3$ ($x=0.1$ and 0.9).

Sample	IS (mm/s)	QS (mm/s)	H (T)	Γ (mm)	Fe Valence
$\text{DyFe}_{0.9}\text{Cr}_{0.1}\text{O}_3$	0.244	0.004	49.516	0.722	Fe(III) HS
$\text{DyFe}_{0.1}\text{Cr}_{0.9}\text{O}_3$	0.216	0.256	/	0.330	Fe(III) HS

IS: isomer shift, QS: quadruple splitting/shift, Γ : Lorentzian linewidth, H: hyperfine

magnetic field, HS: high spin.

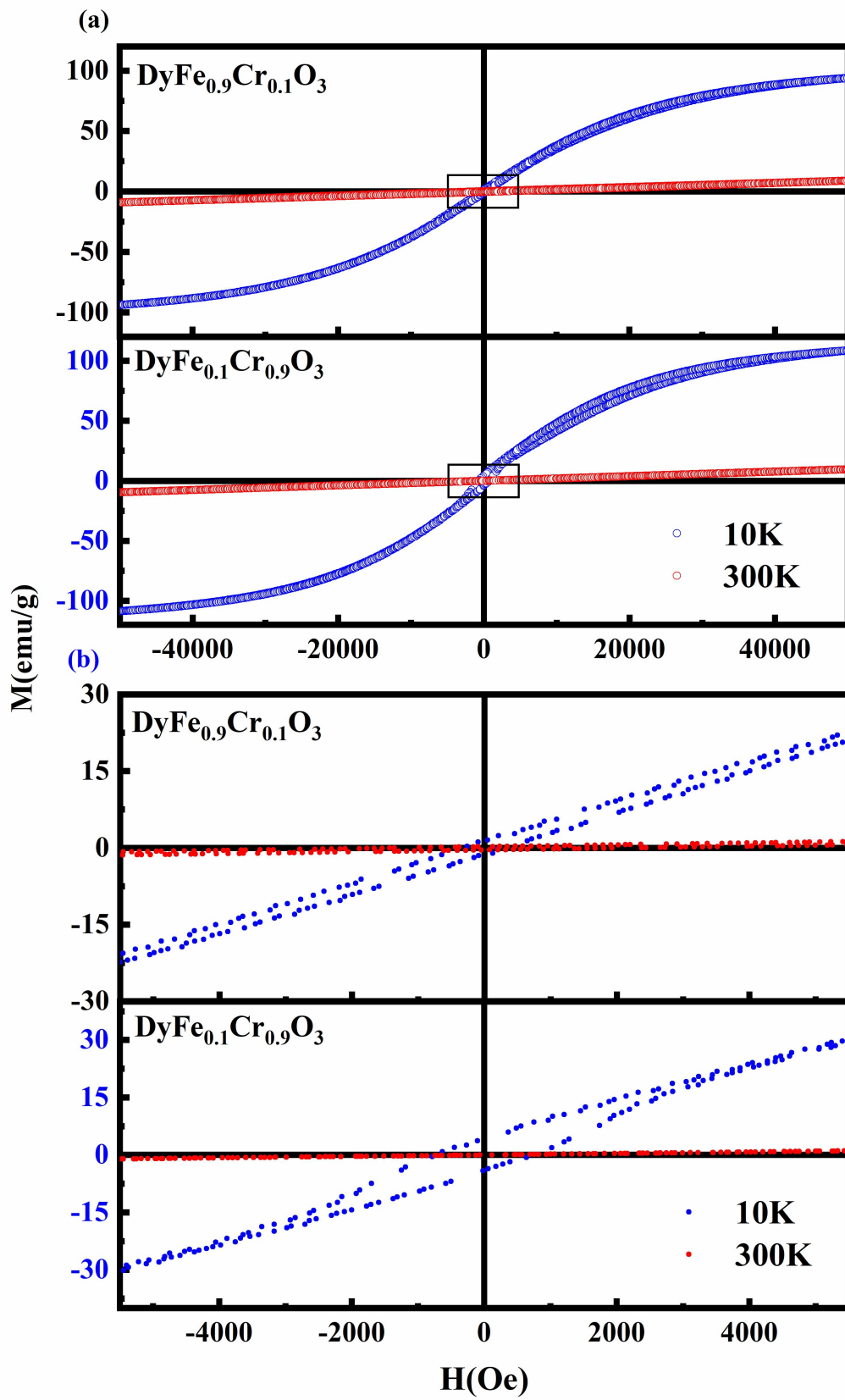


Fig. 3. (a) Magnetization curves of $\text{DyFe}_{1-x}\text{Cr}_x\text{O}_3$ ($x=0.1$ and 0.9) at 10 K and 300 K, respectively. **(b)** The enlarged view of the external magnetic field from -5500 Oe to 5500 Oe.

The Mössbauer spectra of $\text{DyFe}_{1-x}\text{Cr}_x\text{O}_3$ ($x=0.1$ and 0.9) are shown in [Figure 2](#). The Mössbauer spectra at 300 K have obvious differences, which are similar to the general rare-earth iron-chromium perovskites. [\[22,23\]](#) In DFCO with high iron content, the sextet spectrum caused by the hyperfine field can prove its ferromagnetic or antiferromagnetic characteristics. In the samples with high chromium content, the expected doublet state is associated with macroscopic paramagnetism.

The hyperfine parameters fitted by MössWinn 4.0 software are shown in [Table 2](#). In both samples we fit only one iron phase with good results. This also proves the homogeneity of the single phase in the DFCO system. By comparing isomer shift (IS) and quadruple splitting (QS), we believe that Fe ions are in the state of positive trivalent high spin, which will provide an important basis for our subsequent fitting work.

The measurement results of the magnetization curves of the samples are shown in [Figure 3](#). On the whole, the two samples have very similar behaviors under the excitation of the external magnetic field, and the final magnetization is also relatively close. Distinct magnetization processes are observed at 10 K and 300 K, respectively. At 300 K, the magnetization curves of the two samples approached a straight line. The difference is that in the $\text{DyFe}_{0.9}\text{Cr}_{0.1}\text{O}_3$, a very fine hysteresis loop appears, indicating

that an irreversible magnetic component appears in the $\text{DyFe}_{0.9}\text{Cr}_{0.1}\text{O}_3$. According to our previous research on $R\text{Fe}_{1-x}\text{Cr}_x\text{O}_3$ and reference to previous reports, we can understand it as the existence of a weak ferromagnetic phase. Between 300 K and Néel temperature, the spin angle that promotes the reduction of $\text{Fe}^{3+}/\text{Cr}^{3+}$ ions are slightly less than 180° due to the superexchange interaction caused by residual electrons and spin-orbit coupling, and a net magnetic moment appears. Weak ferromagnetic behavior is thus recorded below this temperature. [24] In $\text{DyFe}_{0.1}\text{Cr}_{0.9}\text{O}_3$, however, 300 K has not undergone the Néel phase transition, thus obtaining paramagnetic characteristics. At 10 K, both samples have undergone a Néel phase transition as well as an antiferromagnetic to weak ferromagnetic transition. Therefore, in the magnetization curve at 10 K, both have obvious hysteresis loops, which is the contribution of weak ferromagnetism. But as the temperature decreases, the paramagnetic contribution of Dy^{3+} - Dy^{3+} ($S=5/2$) becomes very large, even enough to mask the weak ferromagnetic contribution of $\text{Fe}^{3+}/\text{Cr}^{3+}$. Especially when the external field is very large, it is difficult to observe the hysteresis loop for both samples, and both show the tendency of paramagnetic magnetization saturation.

Thermomagnetic analysis and Molecular Field Model Fitting

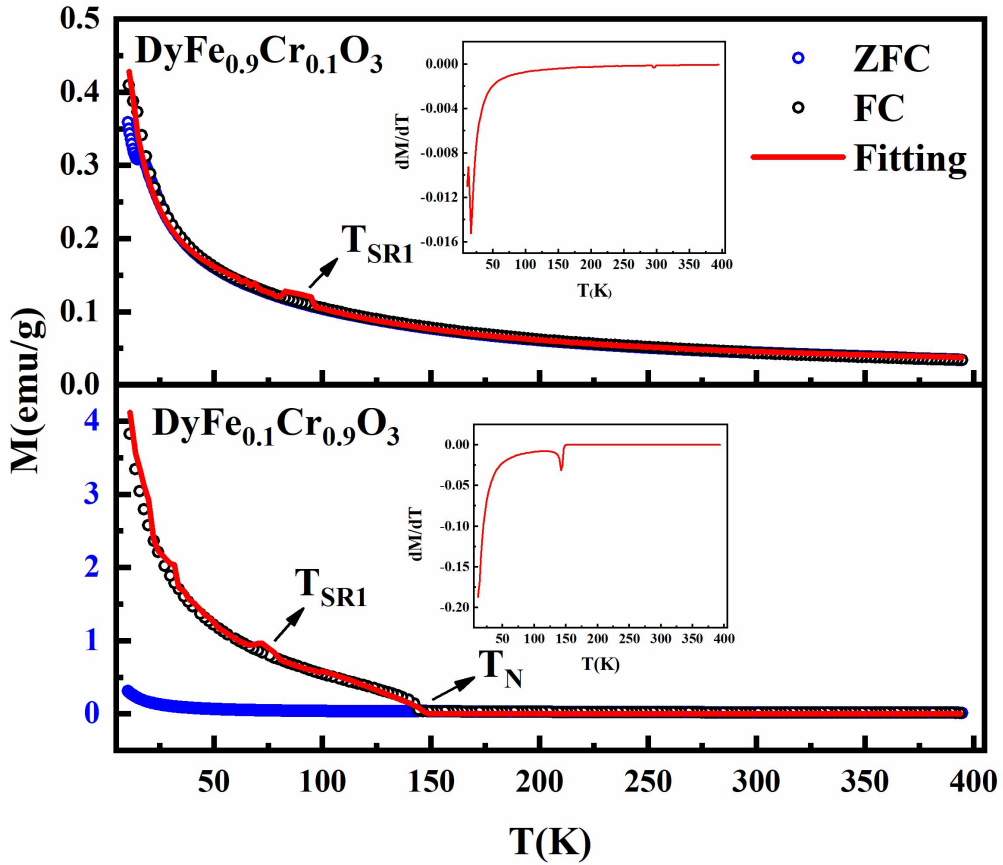


Fig. 4. Thermomagnetic curves and fitting results of $\text{DyFe}_{1-x}\text{Cr}_x\text{O}_3$ ($x=0.1$ and 0.9) in the temperature range from 10 K to 400 K. The inset shows the image of dM/dT vs T .

The field cooling (FC) and zero field cooling (ZFC) curves of DFCO in the temperature range from 10 K to 400 K are shown in [Figure 4](#). In this temperature range, DFCO shows complex magnetic properties. On the whole, FC/ZFC showed an obvious upward trend with the decrease of temperature, but it is obvious that $\text{DyFe}_{0.1}\text{Cr}_{0.9}\text{O}_3$ can finally achieve a larger magnetization, that is to say, the ground state magnetization of $\text{DyFe}_{0.1}\text{Cr}_{0.9}\text{O}_3$ is much larger than that of $\text{DyFe}_{0.9}\text{Cr}_{0.1}\text{O}_3$. This

originates from differences in exchange interactions in the DFCO system. Through the phase transition temperature of pure ferrite and pure chromite in molecular field theory, the exchange constants J_{F-F}/J_{C-C} of $Fe^{3+}-O-Fe^{3+}/Cr^{3+}-O-Cr^{3+}$ can be directly calculated to be -25.8 K and -6 K, respectively. Therefore, the exchange that is strongly related to the low-temperature magnetization is not the exchange of $Fe^{3+}-O-Fe^{3+}/Cr^{3+}-O-Cr^{3+}$, but the exchange between B site ions and A being rare earth ions, that is, $Dy^{3+}-O-Fe^{3+}/Dy^{3+}-O-Cr^{3+}$.

To observe the magnetic phase transition of the two samples over the entire temperature range, we plotted the change in dM/dT vs T (Illustrations in Figure 4.). It is found that the $DyFe_{0.9}Cr_{0.1}O_3$ still maintains a weak magnetization in the whole temperature range, and no obvious Néel temperature point is observed. In $DyFe_{0.1}Cr_{0.9}O_3$, a very obvious magnetic transition occurs at about 147 K, and the magnetization is almost zero above this temperature, and the paramagnetic characteristics are very obvious. This also corresponds to the result of the Mössbauer spectrum. Two samples also have a very obvious magnetic phase transition point at very low temperature. Based on previous literature, this should not be the phase transition point where the Dy^{3+} ion interacts with itself, but more likely the phase transition point where the interaction with the B-site ion occurs. This is because the antiferromagnetic phase transition of $Dy^{3+}-Dy^{3+}$ is at a much lower temperature (about 5 K).

In order to gain a more accurate understanding of the intrinsic origin of the magnetic properties of DFCO, a simple approximate simulation of the system is

carried out using a four-sublattice molecular field model. In this process we consider only the exchange interactions in $\text{Dy}^{3+}\text{-Fe}^{3+}$, $\text{Dy}^{3+}\text{-Cr}^{3+}$, $\text{Fe}^{3+}\text{-Fe}^{3+}$, $\text{Cr}^{3+}\text{-Cr}^{3+}$, $\text{Fe}^{3+}\text{-Cr}^{3+}$, the reason for omitting the $\text{Dy}^{3+}\text{-Dy}^{3+}$ exchange interactions is that the paramagnetic contribution is very large over the whole simulated temperature range.

For $\text{DyFe}_{0.9}\text{Cr}_{0.1}\text{O}_3$, the mean field is expressed as:

$$H_{\text{Dy}} = \lambda_{\text{DyCr}}M_{\text{Cr}} + \lambda_{\text{DyFe}^b}M_{\text{Fe}^b} + \lambda_{\text{DyFe}^a}M_{\text{Fe}^a} + h \quad (2)$$

$$H_{\text{Fe}^a} = \lambda_{\text{Fe}^a\text{Fe}^b}M_{\text{Fe}^b} + \lambda_{\text{Fe}^a\text{Cr}}M_{\text{Cr}} + \lambda_{\text{Fe}^a\text{Dy}}M_{\text{Dy}} + h \quad (3)$$

$$H_{\text{Fe}^b} = \lambda_{\text{Fe}^b\text{Fe}^a}M_{\text{Fe}^a} + \lambda_{\text{Fe}^b\text{Dy}}M_{\text{Dy}} + h \quad (4)$$

$$H_{\text{Cr}} = \lambda_{\text{CrFe}^a}M_{\text{Fe}^a} + \lambda_{\text{CrDy}}M_{\text{Dy}} + h \quad (5)$$

For $\text{DyFe}_{0.1}\text{Cr}_{0.9}\text{O}_3$, the mean field is expressed as:

$$H_{\text{Dy}} = \lambda_{\text{DyFe}}M_{\text{Fe}} + \lambda_{\text{DyCr}^b}M_{\text{Cr}^b} + \lambda_{\text{DyCr}^a}M_{\text{Cr}^a} + h \quad (6)$$

$$H_{\text{Cr}^a} = \lambda_{\text{Cr}^a\text{Cr}^b}M_{\text{Cr}^b} + \lambda_{\text{Cr}^a\text{Fe}}M_{\text{Fe}} + \lambda_{\text{Cr}^a\text{Dy}}M_{\text{Dy}} + h \quad (7)$$

$$H_{\text{Cr}^b} = \lambda_{\text{Cr}^b\text{Cr}^a}M_{\text{Cr}^a} + \lambda_{\text{Cr}^b\text{Dy}}M_{\text{Dy}} + h \quad (8)$$

$$H_{\text{Fe}} = \lambda_{\text{FeCr}^a}M_{\text{Cr}^a} + \lambda_{\text{FeDy}}M_{\text{Dy}} + h \quad (9)$$

where λ_{ij} represents the molecular field constant between sublattice i and sublattice j , and it is positively related to the exchange constant J_{ij} , h is the external magnetic field, and M_i is the magnetisation intensity of sublattice i . M_i can be expressed as:

$$M_i = \chi_i N_A g \mu_B S_i B_{S_i} \left(\frac{g \mu_B S_i H_i}{k_B T} \right) \quad (10)$$

Where χ_i is the molar quantity of i ions, g is the lande factor, and μ_B represents the Bohr magneton. N_A is the Avogadro constant. S_i is the spin quantum number of i ions ($S_{\text{Fe}} = 5/2$, $S_{\text{Cr}} = 3/2$, $S_{\text{Dy}} = 5/2$). The exchange constant J_{MM} between M and M

ions can be calculated by:

$$|J_{MM}| = \frac{2Z_{MM}S_M(S_M + 1)}{3k_B T_N^M} \#(11)$$

With this equation we can understand that once the corresponding Néel temperatures for rare-earth ferrites and chromium oxides are obtained, we can calculate the corresponding approximate exchange constants. Based on previous studies, we find that the phase transition temperatures of DyFeO₃ and DyCrO₃ are approximately 645 K and 150 K, respectively, with corresponding exchange constants of -25.8 K and -6 K for J_{F-F} and J_{C-C} , respectively. Thus the magnetisation intensity at each temperature point can be obtained by means of equations (2) - (10). The algorithm used for the fitting is the latest Marine Predator Algorithm (MPA). [24]

At the same time, we define the effective spin of the A-site rare earth ion as the projection of its total spin onto the B-site spin plane. This is different from the research methods of many previous scholars. Before this, most researchers generally defined the spin of A-site rare earth ions as a constant, and did not think it was changing. However, during the fitting process, we found that in addition to the spin reorientation of the Fe³⁺/Cr³⁺ ions at the B site, the spins of the A-site ions also changed at the same time, and the final error was very small. This work has been well validated in Nd, Pr, Er rare earth perovskites. In the high temperature section, the influence of the spin of rare earth ions on the magnetization is almost negligible, so the high temperature section is selected to first fit to obtain the relevant exchange constants (in Table. 3). The obtained exchange constants are then used to fit the A-site effective spins over the entire temperature range. The thermomagnetic curve after

junction fitting is shown as the red line in [Figure. 4](#).

It can be seen that the fitting is very good, and the error can even be less than 10^{-3} at some temperature points, and only slightly larger errors appear in some temperature ranges. Around 75 K, the fitted curves for both samples exhibited slightly larger errors. In many literatures, [\[7,12, 22, 25,26\]](#) 75 K is a very specific temperature point, the time at which the B-site spin reorientation occurs. In the original data, the spin of the Dy^{3+} ion will have a huge effect on the whole system due to the decrease in temperature, i.e. a very large paramagnetic shielding. In the experimental data, the paramagnetic effect far exceeds the contribution of weak ferromagnetism, so it is difficult to observe the magnetization change due to the B-site spin reorientation. In the fitting process, this detail is clearly manifested. In addition, we found that in the ZFC curve of $DyFe_{0.9}Cr_{0.1}O_3$, there is an obvious turning point at about 15 K, which is probably the phase transition temperature point where Dy^{3+} ions are coupled with Fe^{3+}/Cr^{3+} ions. While in $DyFe_{0.1}Cr_{0.9}O_3$, this process may be below 10 K without being observed.

The fitted effective spin of Dy^{3+} ions as a function of temperature is shown in [Figure. 5](#). The corresponding Dy^{3+} spin direction and the angle between the Fe^{3+}/Cr^{3+} spin plane is also reflected.

Table. 3. Exchange constant of $DyFe_{1-x}Cr_xO_3$ ($x=0.1$ and 0.9).

Sample	J_{F-F}	J_{C-C}	J_{F-C}	J_{D-F}	J_{D-C}
$DyFe_{0.9}Cr_{0.1}O_3$	-25.800	-6.000	-12.214	-5.119	-11.385

DyFe _{0.1} Cr _{0.9} O ₃	-25.800	-6.000	-10.439	-2.005	-5.537
------------------------------------------------------	---------	--------	---------	--------	--------

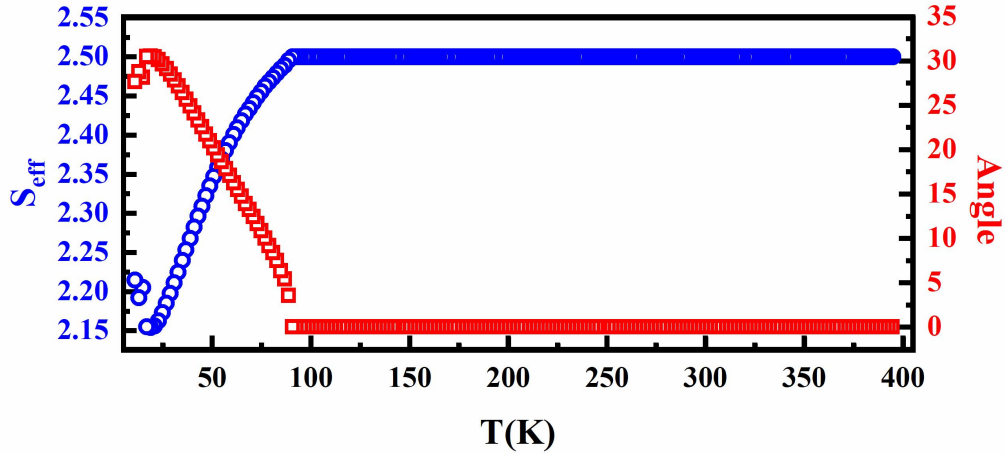


Fig. 5. The effective spins of Dy³⁺ ions and the corresponding angle with the Fe³⁺/Cr³⁺ spin plane change with temperature.

Conclusions

In summary, Mössbauer spectroscopy and magnetic measurements were performed on single-phase DyFe_{0.9}Cr_{0.1}O₃ and DyFe_{0.1}Cr_{0.9}O₃ prepared by a simple sol-gel method. The Mössbauer spectra at room temperature are consistent with the results shown by the magnetization curves, showing weak ferromagnetic properties in DyFe_{0.9}Cr_{0.1}O₃ and obvious paramagnetic behavior in DyFe_{0.1}Cr_{0.9}O₃. At 10 K, both samples have crossed the antiferromagnetic to weak ferromagnetic transition temperature, but the magnetization curves will tend to paramagnetic saturation due to the action of high-spin Dy³⁺ ions under a large external magnetic field.

By fitting the molecular field model of the four-sublattice and MPA algorithm, the thermomagnetic curve with a high degree of fit is obtained, and the relevant exchange constants are obtained. Different from past theories, we define the effective spin of rare earth ions at the A site as the projection of its full spin on the spin plane at the B site, and fit it as an unknown parameter over the entire temperature range, and finally get the effective spin about temperature change relationship.

Conflicts of interest

There are no conflicts to declare.

Data Availability

The datasets generated and/or analysed during the current study are available from the corresponding author on reasonable request.

Acknowledgements

This work was supported by National Natural Science Foundation of China (grant number 12105137, 62004143), the Central Government Guided Local Science and Technology Development Special Fund Project (2020ZYYD033), the National Undergraduate Innovation and Entrepreneurship Training Program Support Projects of China, the Natural Science Foundation of Hunan Province, China (grant number S202110555177), the Natural Science Foundation of Hunan Province, China (grant number 2020JJ4517), Research Foundation of Education Bureau of Hunan Province, China (grant number 19A433, 19C1621).

References

[1] Y. M. Cao, S. X. Cao, W. Ren, Z. J. Feng, S. J. Yuan, B. J. Kang, B. Lu, J. C.

- Zhang, *Appl. Phys. Lett.* **104**, 232405 (2014).
- [2] C. Lyu, C. Liu, H. H. Min, X. Y. Shi, R. Jiang, Z. K. Ao, X. Zhang, C. L. Wang, H. F. Ma, *J. Alloys Compd.* **913**, 165300 (2022).
- [3] Z. Shi, J. Guo, Y. Chen, Q. Li, Y. Pan, H. Zhang, Y. Xia, W. Huang, *Adv. Mater.* **29**, 1605005 (2017).
- [4] G. Chen, Y. Zhu, H. M. Chen, Z. Hu, S. F. Hung, N. Ma, J. Dai, H. J. Lin, C. T. Chen, W. Zhou, Z. Shao, *Adv. Mater.* **31**, e1900883 (2019).
- [5] F. Polo-Garzon, Z. Wu, *J. Mater. Chem. A* **6**, 2877 (2018).
- [6] A. Kostopoulou, E. Kymakis, E. Stratakis, *J. Mater. Chem. A* **6**, 9765 (2018).
- [7] H. L. Wu, S. X. Cao, M. Liu, Y. M. Cao, B. J. Kang, J. C. Zhang, W. Ren, *Phys. Rev. B* **90**, 144415 (2014).
- [8] H. Park, A. J. Millis, C. A. Marianetti, *Phys. Rev. Lett.* **109**, 156402 (2012).
- [9] A. Najev, S. Hameed, D. Gautreau, Z. Wang, J. Joe, M. Požek, T. Birol, R. M. Fernandes, M. Greven, D. Pelc, *Phys. Rev. Lett.* **128**, 167201 (2022).
- [10] A. Somvanshi, A. Ahmad, S. Husain, S. Manzoor, A. A. A. Qahtan, N. Zarrin, M. Fatema, W. Khan, *Appl. Phys. A: Mater. Sci. Process* **127**, 424 (2021).
- [11] J. P. Bolletta, F. Pomiro, R. D. Sánchez, V. Pomjakushin, G. Aurelio, A. Maignan, C. Martin, R. E. Carbonio, *Phys. Rev. B* **98**, 134417 (2018).
- [12] M. H. Mohammed, J. Horvat, Z. X. Cheng, S. X. Cao, E. Y. Li, R. B. Li, *J. Phys. Chem. C* **123**, 30584 (2019).
- [13] G. B. Song, J. J. Jiang, B. J. Kang, J. C. Zhang, Z. X. Cheng, G. H. Ma, S. X. Cao, *Solid State Commun.* **211**, 47 (2015).

- [14] J. S. Zhang, R. B. Li, X. X. Ma, X. Luo, Y. K. Chen, B. J. Kang, J. C. Zhang, S. X. Cao, *Ceram. Int.* **46**, 23556 (2020).
- [15] S. A. Nikitin, K. P. Skokov, Yu. S. Koshkid'ko, Yu. G. Pastushenkov, T. I. Ivanova, *Phys. Rev. Lett.* **105**, 137205 (2010).
- [16] J. Y. Shen, J. J. Mo, Z. Y. Lu, C. Y. Gong, Z. J. Wu, K. Y. Gao, M. Liu, Y. F. Xia, *Chem. Phys. Lett.* **806**, 139991 (2022).
- [17] J. Y. Shen, J. J. Mo, Z. Y. Lu, Z. J. Wu, C. Y. Gong, K. Y. Gao, P. L. Zheng, M. Liu, Y. F. Xia, *NANO*, doi: 10.1142/S1793292022500801.
- [18] J. Y. Shen, J. J. Mo, Z. Y. Lu et al. Unraveling the nature of thermally induced spin reorientation in $\text{NdFe}_{1-x}\text{Cr}_x\text{O}_3$ [J]. arXiv preprint arXiv:2207.03646, 2022.
- [19] J. Y. Shen, J. J. Mo, Z. Y. Lu et al. Unraveling Thermally Induced Spin reorientation of Strongly Disordered $\text{NdFe}_{0.5}\text{Cr}_{0.5}\text{O}_3$ System[J]. arXiv preprint arXiv:2207.03220, 2022.
- [20] T. V. Aksenova, Sh. I. Elkalashy, A. S. Urusova, V. A. Cherepanov, *Russ. J. Inorg. Chem+* **62**, 1090 (2017).
- [21] J. J. Mo, M. Liu, S. Y. Xu, P. Y. Xia, Q. H. Zhang, J. Y. Shen, Y. F. Xia, *Ceram. Int.* **48**, 31309 (2022).
- [22] S. Shravan Kumar Reddy, N. Raju, Ch. Gopal Reddy, P. Yadagiri Reddy, K. Rama Reddy, V. Raghavendra Reddy, *J. Magn. Magn. Mater.* **396**, 214 (2015).
- [23] W. Yi, Y. Matsushita, Y. Katsuya, K. Yamaura, Y. Tsujimoto, I. A. Presniakov, A. V. Sobolev, Y. S. Glazkova, Y. O. Lekina, N. Tsujii, S. Nimori, K. Takehana, Y. Imanaka, A. A. Belik, *Dalton Trans.* **44**, 10785 (2015).

[24] A. Faramarzi, M. Heidarinejad, S. Mirjalili, A. H. Gandomi, *Expert. Syst. Appl.* **152**, 113377 (2020).

[25] C. L. Li, S. S. Zheng, G. O. Barasa, Y. F. Zhao, L. Wang, C. L. Wang, Y. Lu, Y. Qiu, J. B. Cheng, Y. S. Luo, *Ceram. Int.* **47**, 35160 (2021).

[26] B. Rajeswaran, D. Sanyal, Mahuya Chakrabarti, Y. Sundarayya, A. Sundaresan, C. N. R. Rao, *EPL* **101**, 17001 (2013).